Journal of Colloid and Interface Science 650 (2023) 1174–1181

Contents lists available at ScienceDirect

Journal of Colloid And Interface Science

journal homepage: www.elsevier.com/locate/jcis

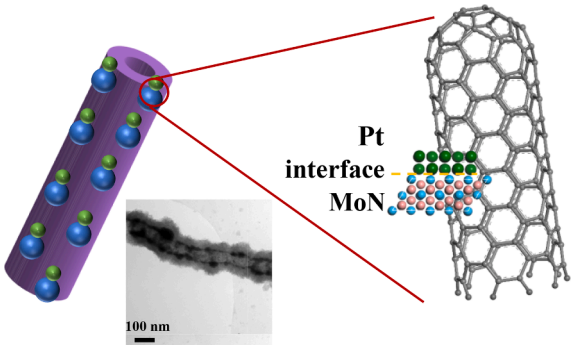
Carbon nanotubes encapsulating Pt/MoN heterostructures for superior hydrogen evolution

Peijia Wang, Yaotian Yan, Bin Qin, Zhenyu Ye, Wei Cai, Xiaohang Zheng *

School of Materials Science and Engineering, Harbin Institute of Technology, Harbin 150001, China

GRAPHICAL ABSTRACT

We fabricated PtNi/MoN@C heterostructured catalysts on nanotubes by in situ precursor conversion strategies, enhancing the electron transport and reduce the $\triangle G_{H^*}$ and showing prominent electrochemical performance.



ARTICLE INFO

Keywords:
N doped carbon nanotubes
MoN nanoparticles
Pt doping
Heterostructures
Hydrogen evolution reaction

ABSTRACT

Achieving efficient hydrogen evolution reaction (HER) catalysts to scale up electrochemical water splitting is desirable but remains a major challenge. Here, nitrogen-doped carbon nanotubes (NCNTs) loaded with PtNi/MoN electrocatalyst (PtNi/MoN@C) is synthesized by a simple strategy to obtain stronger interphase effects and significantly improve HER activity. The surface morphology of the materials is altered by Pt doping and the electronic structure of MoN is changed, which optimizing the electronic environment of the materials, shifting the binding energy and giving the materials a higher electrical conductivity, this ultimately leads to faster proton and electron transfer processes. The synergistic effect of Pt nanoparticles, MoN and the good combination with carbon leads to a high HER activity of 18 mV to reach 10 mA cm^{-2} in alkaline solution, outperforming that of the commercial Pt/C. Theoretical studies show that the heterostructures can efficiently enhance the electron transport and reduce the $\triangle G_{H^*}$.

* Corresponding author.
E-mail address: zhengxiaohang@hit.edu.cn (X. Zheng).

https://doi.org/10.1016/j.jcis.2023.07.039
Received 22 May 2023; Received in revised form 4 July 2023; Accepted 7 July 2023
Available online 8 July 2023
0021-9797/© 2023 Published by Elsevier Inc.

1. Introduction

Hydrogen energy from electrochemical water splitting as one of the most promising means of clean energy production has attracted much attention, the key to which lies in the selection of suitable catalysts to reduce overpotentials and increase yield [1–3]. The noble metal catalysts currently used in industrial applications have excellent performance but the high price impedes the large-scale application [4,5].

Transition metal materials with easily tunable electronic structures that can meet the industrial demand for low-cost applications are abundant and inexpensive in the earth's crust [6–8]. Compared with other transition metals such as iron and cobalt, transition metal nickel based materials have good stability and corrosion resistance in alkaline media and become the most investigated materials for HER electrocatalysts [9,10]. Compared to single metal systems, the catalyst with binary or multiple self-supporting nanostructures can further tune the electronic properties and adsorption energy of the reaction intermediates and improve the catalytic activity by exploiting the synergistic interaction between metal cations with different d-band centers [11–14]. Among them, molybdenum nitride (MoN) has a unique structure in which the nitrogen atoms occupy interstitial positions in the metal lattice, providing good metallic conductivity and mechanical stability [15]. In addition, the introduction of metal-nitrogen bonds expands the original lattice while reducing the d-band contraction, which has a higher density of states close to the metal Fermi level, giving MoN catalytic activity similar to that of noble metals [16,17]. Therefore, MoN with a strong hydrogen bonding energy can combine with weaker metals to give a relatively moderate value. According to the "volcano diagram", there is a correlation between HER activity and hydrogen-metal bonding strength [18]. Based on the above concept, it is worth to exploit the synergistic effect between transition metal and MoN electrocatalysts to achieve excellent HER activity. For example, Liu et al. [19] designed Ni nanoparticles embedded MoN microrods cultured on roughened nickel sheet (Ni/MoN/rNS) to exhibit excellent catalytic performance in HER with an overpotential as low as 67 mV at current density of -10 mA cm^{-2}.

To further enhance the activity and stability of HER electrocatalysts, transition metal-based compounds are often immobilized on various conductive substrates such as covalent organic frameworks [20], carbon nanosheets [21] and carbon nanotubes [22], which not only prevent aggregation of transition metal-based compounds but also increase the dispersion of active sites [23,24]. Among these, carbon nanotubes are a promising catalyst support due to their large specific surface area, high mechanical strength, good electrical conductivity and tunable physical/chemical properties[25]. A large number of researchers have combined carbon nanotubes with nanostructures to obtain electrocatalysts with superior performance. For example, Cheng et al.[26] proposed a nanocomposite containing MoN nanoparticles (3–5 nm) and B,N conjugated carbon nanotubes with diameters of 30–50 nm (denoted as h-MoN@BNCNT). The high surface area (226 m^2 g^{-1}) and more active sites in the prepared h-MoN@BNCNT gave the nanocomposite effective electrocatalytic properties. The design of MoN-based catalysts with tailored structures and efficient catalytic activity for alkaline electrochemical water splitting is of great interest, although the research is still quite limited.

In this work, we have designed and prepared nitrogen-doped carbon nanotubes (NCNTs) loaded with PtNi/MoN heterostructured catalysts (denoted as PtNi/MoN@C) by in situ precursor conversion strategies. The generation of NCNTs is facilitated by high temperature using Ni as catalyst, while MoN nanoparticles are dispersed in NCNTs, followed by a simple impregnation method to obtain PtNi/MoN@C. The synergistic effect of Pt nanoparticles, MoN and the good combination with NCNTs leads to a high HER activity of 18 mV to reach -10 mA cm^{-2} in alkaline solution. Theoretical studies show that the heterostructure can efficiently enhance the electron transport and reduce the $\triangle G_{H^*}$, and then improve the electrocatalytic performance.

2. Experimental section

Materials: All the chemicals including $Ni(NO_3)_2{\cdot}6H_2O$ (99%), $Na_2MoO_4{\cdot}2H_2O$ (AR, 99%), 5% Nafion solution (Nafion®117 solution), dicyandiamide (98%), hydrochloric acid (37 a.t.%), ethanol (95%) and chloroplatinic acid (99%) were purchased from Macklin Reagents and used directly without further purification. Pt/C powder (Pt 20 w.t.%, powder) was purchased from Zhongke Innovation Energy Technology Co..

Before material preparation, Ni foam was pretreated in advance: soaked in hydrochloric acid solution for 5 min, then washed with ethanol and deionized water several times and placed in a vacuum oven to dry at 60 °C. The Ni foam was purchased from Jia Yisheng Co., Ltd. (Kun Shan); the thickness was 1.5 mm, the surface density was 600 g/m^2 and the hole number was 110 ppi. The size of all the sample used in test was 1*1 cm^2.

2.1. Synthesis of NiMo-O

Solving 0.5 mmol of $Ni(NO_3)_2{\cdot}6H_2O$ and 0.5 mmol of $Na_2MoO_4{\cdot}2H_2O$ in 80 mL of deionized water, after the drug is completely dissolved, it was transferred into a 100 mL Teflon-lined stainless autoclave and put the prepared Ni foam (2*4 cm^2) completely in the solution and react at 120 ℃ for 8 h, then washed several times with ethanol and deionized water and dried at 60 ℃. Then samples was placed in tube furnace and calcined under air. The temperature was raised to 400 ℃ at a rate of 2 ℃ min^{-1} and kept for 2 h, then naturally cooled to room temperature. The product was labeled NiMo-O.

2.2. Synthesis of Ni/MoN@C

The NiMo-O precursors were treated in a tube furnace in nitrogen atmosphere using dicyandiamide as the carbon and nitrogen source. The dicyandiamide and the NiMo-O sample were placed in the upstream and downstream of the tube furnace, respectively, and the temperature was raised to 800 ℃ and maintained for 2 h. The product was labeled Ni/MoN@C. For comparison, the amount of carbon/nitrogen source was adjusted to 150 mg, 200 mg, 300 mg and 350 mg of dicyandiamide, while the treatment temperatures were 700, 800 and 850 ℃, respectively.

2.3. Synthesis of PtNi/MoN@C

The chloroplatinic acid solution with a concentration of 1 mg μL^{-1} was selected, 3, 5 and 8 μL of chloroplatinic acid solution were added to 20 mL of ethanol, ultrasonicated for 2 min and the Ni/MoN@C sample (1×2 cm^2) was completely immersed in the configured solution, then held at 80 °C for 20 min, washed several times with ethanol and dried at 60 °C. Then the sample was annealed in argon at 400 °C for 1 h to obtain the PtNi/MoN@C.

Commercial Pt/C electrode was prepared with the 20 w.t.% Pt/C powder and 5 w.t.% Nafion solution in ethanol and then uniformly dispersed on the Ni foam and dried at 60 ℃ with the loading of ~ 0.5 mg cm^{-2}.

2.4. Materials Characterization

The fabricated electrocatalysts were characterized by SEM (Merlin Compact field emission scanning electron microscope), TEM (Talos F200X transmission electron microscope), XRD (Empyrean X-ray diffractometer), Raman spectroscopy (Optosky ATR8300 with 532 nm excitation) and XPS (ESCALAB 250Xi X-ray photoelectron spectrometer) to analyze their microstructure and composition. Elemental content measured by inductively coupled plasma spectrometry (ICP-OES 7400, Thermo).

2.5. Electrochemical Test

Electrochemical performance measurement mainly include linear voltammetry curve (LSV), cyclic voltammetry scan (CV), AC impedance test (EIS), timing potential analysis, etc. were measured in the electrochemical workstation (CHI 760E). In HER test, a conventional three-electrode system was used, in which graphite rod was used for the opposite electrode, Hg/HgO electrode was used for the reference electrode, and 1 M KOH aqueous solution was used as the electrolyte. All voltage values were iR compensated and converted to standard hydrogen electrode potential.

3. Result and discussion

As shown in Fig. 1, the NiMo-O nanosheets are first prepared on Ni foam substrate by hydrothermal reaction and then annealed in air at 400 °C to produce NiMo-O nanosheets with flower-like flake structure. The CVD process is carried out in nitrogen atmosphere as shown in the schematic diagram. When the heat treatment temperature reaches 600 °C, the CN_x gas generated from the decomposition of dicyandiamine reacts with the NiMo-O nanosheets to reduce the Ni in NiMo-O, and the initial NiMo-O is converted to Ni/MoO_x in the reducing atmosphere. When the temperature is further increased to 800 °C, MoO_x will then continue to absorb CN_x gas and be nitrided in situ to form MoN, while in this process the in situ reduced Ni nanoparticles act as catalytic center and use CN_x as a carbon source to form NCNTs (the product denoted as Ni/MoN@C)[27]. The formed Ni/MoN@C is then dispersed in an ethanolic solution of H_2PtCl_6 using a chemical bath and heat treatments to obtain PtNi/MoN@C. SEM results in Fig. 2a shows that after hydrothermal reaction and oxidation treatment, the Ni foam substrate is completely covered with NiMo-O flower-like nanosheets in a uniform and dense manner. After the CVD treatment, the morphology of the flower-like NiMo-O nanosheets changed. The formation of a large number of Ni/MoN nanoparticles inside the interwoven NCNTs was shown in Fig. 2b. SEM images of Ni/MoN@C with different dicyandiamide content and different temperature in CVD process is shown in Fig. S1 and S3 and tested LSV curves shown in Fig. S2 and S4. The cross-linked NCNTs structure changes to a granular structure after Pt doping in Fig. 2c, which is due to the etching effect of chloroplatinic acid and the aggregation of NCNTs loaded nanoparticles to a certain extent. EDS in Fig.S5 shows a homogeneous distribution of Mo, N and Pt elements and LSV curves of different chloroplatinic acid content were shown in Fig. S6.

The prepared samples are further analyzed by XRD. As shown in Fig. 2d, the sample is located at 26.4° corresponding to carbon peak and located at 31.9°, 36.2°, 49.0°, 65.1° and 74.3° corresponding to (002), (200), (202), (220)and (222) planes of MoN (PDF# 25–1367). After Pt doping, the corresponding metal Pt peak can be detected at 39.8° that is (111) crystal plane of metal Pt. As shown in Fig. 2e, the Raman characteristic peaks at 1350 and 1580 cm^{-1} correspond to the D peak of disordered carbon and the G peak of graphitic carbon, respectively. The high ratio of the D peak to the G peak (I_D/I_G) of PtNi/MoN@C (1.16) and Ni/MoN@C (1.13) indicates the presence of a large number of defects in the NCNTs, which is due to the presence of a large number of N atoms doped in the NCNTs [28].

Further insights into the morphology and structure of the as-prepared samples are elucidated by TEM and HRTEM. The TEM results further show that the MoN nanoparticles are wrapped by interwoven NCNTs, and in agreement with the SEM results, as shown in Fig. 3a and 3b . The in situ grown NCNTs are also interwoven with each other and the nanoparticles are distributed over the NCNTs to form horizontal conducting pathways between the nanoparticles, ensuring long distance electron transport through the materials. As shown in Fig. 3c and S9, the MoN nanoparticles are analyzed by HRTEM with a crystalline spacing of 0.186 nm corresponding to the (202) crystalline plane of MoN, while a crystalline spacing of 0.23 nm corresponding to the Pt (111) crystalline plane. According to the above experimental results, Pt nanoparticles are tightly embedded in NCNTs and grafted onto MoN nanoparticles, and the average particle size of Pt is 5–15 nm. As shown in Fig. 3d, the Ni nanoparticles are encapsulated in bamboo-like NCNTs, and further show that the crystal plane spacing of 0.199 nm corresponding to the (111) crystal plane of Ni. This also indicates that Ni act as a catalyst for NCNTs. This result is also consistent with the elemental distribution in Fig. 3e, which shows the corresponding element mapping distribution.

The surface composition and chemical states of the samples are further investigated by XPS. The presence of the elements Pt, Mo, O, C and N in the prepared PtNi/MoN@C is evident from the XPS as shown in Fig. 4. The C 1 s XPS spectra in Fig. 4a has three dividing peaks, representing C—C (284.8 eV), C—O (285.8 eV) and C═O (288.2 eV). The O 1 s spectrum in Fig. 4b can be divided into four peaks, O1 at 530.06 eV, O2 at 530.85 eV, O3 at 531.56 eV and O4 at 532.40 eV. Fig. 4c shows the XPS spectra of Mo 3d in the material, the two peaks corresponding to binding energies of 229.1 eV and 232.2 eV are shown for Mo^{5+} (229.1 and 232.2 eV)[29]. Among them, Mo^{4+} (229.7 and 232.8 eV) and Mo^{6+} (232.3 and 235.4 eV) peaks are due to oxidation caused by exposure to

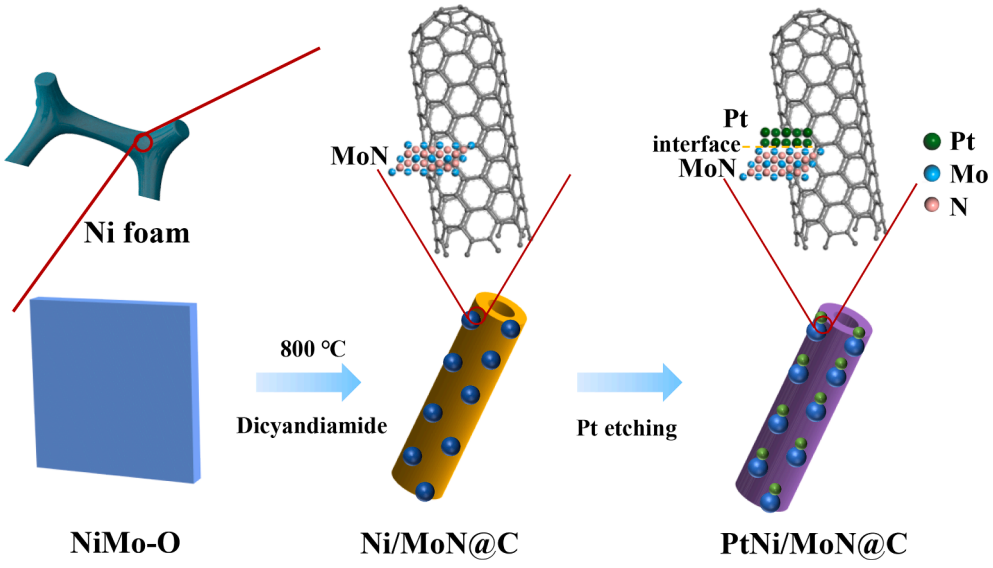


Fig. 1. Schematic illustration of the fabrication of PtNi/MoN@C.

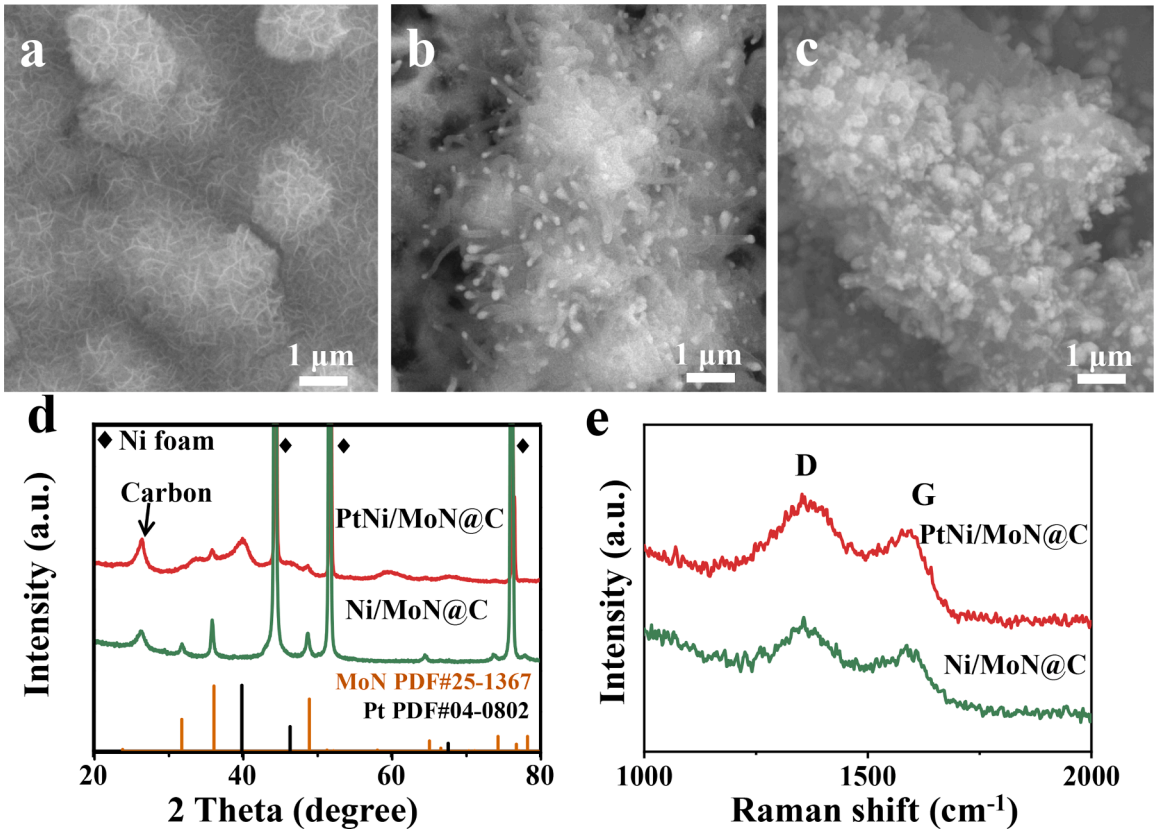


Fig. 2. SEM images of: (a) NiMo-O, (b) Ni/MoN@C and (c) PtNi/MoN@C. (d) XRD patterns of the obtained catalysts. (e) Raman spectra of the obtained catalysts.

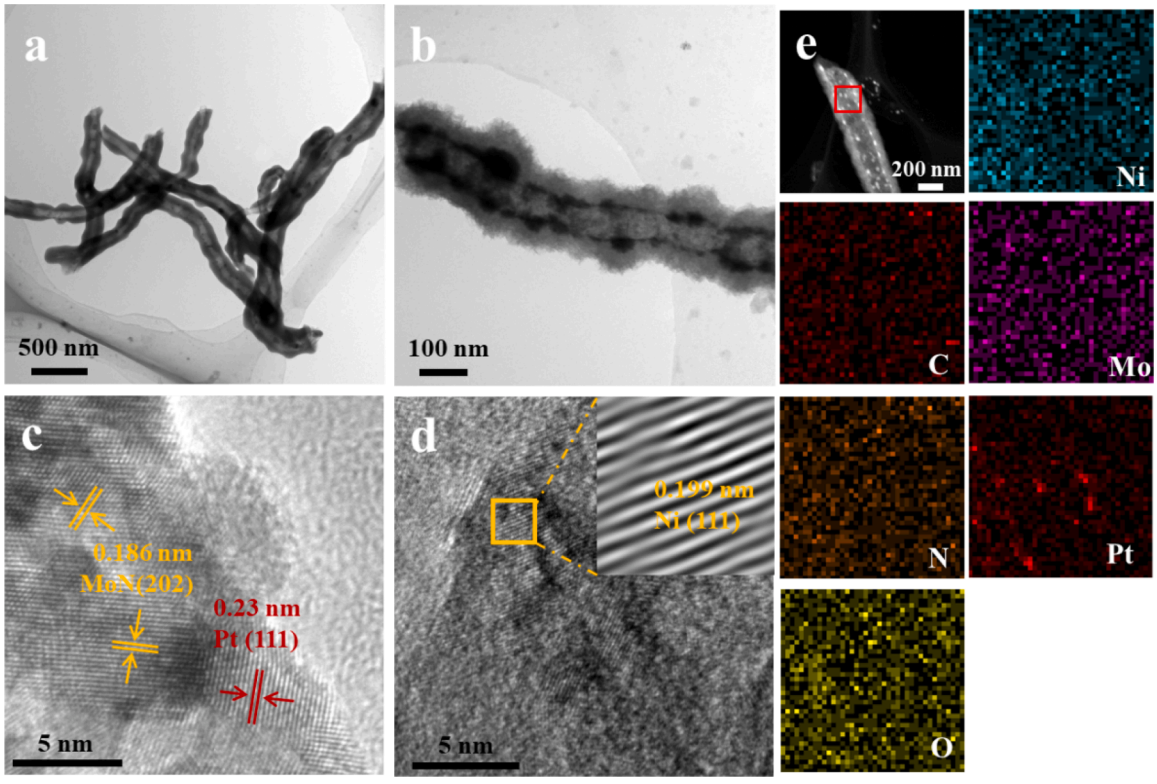


Fig. 3. (a)-(d) TEM image and HRTEM image of PtNi/MoN@C. (e) TEM mapping of PtNi/MoN@C.

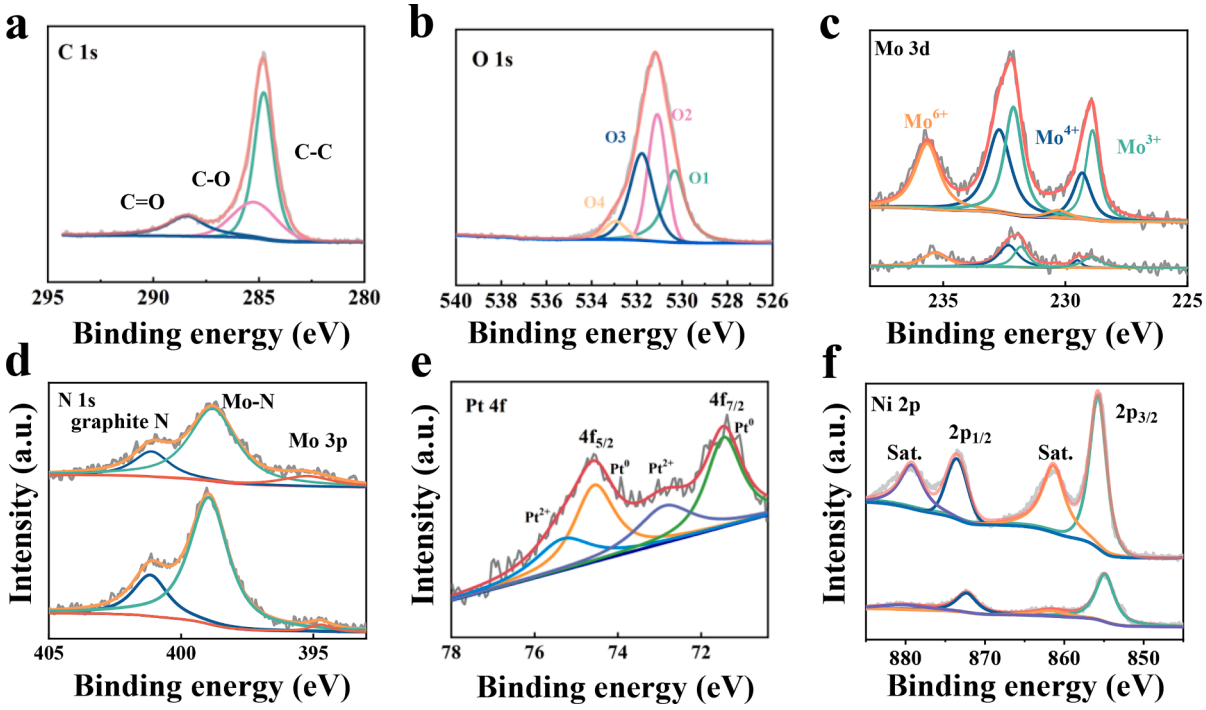


Fig. 4. XPS spectra of (a) C 1s, (b) O 1s, (c) Mo 3d, (d) N 1s, (e) Pt 4f and (f) Ni 2p for Ni/MoN@C and PtNi/MoN@C.

air [8,30]. For the N 1 s spectrum, the peak at 394.9 eV is assigned to Mo 3p, due to the partial overlap of Mo 3p and N 1 s [31]. The other two peaks at 398.6 and 400.8 eV can be assigned to *N*-Mo and N—H, respectively. Where N —H probably comes from the reaction of surface N and H_2 during the Ni/MoN synthesis, which accelerates the electrocatalytic process to some extent [32]. The high-resolution Pt 4f spectra (Fig. 4e) can be fitted to Pt $4f_{7/2}$ (71.3 eV and 74.65 eV) and Pt $4f_{5/2}$ (72.6 eV and 75.58 eV), matching to Pt^0 and Pt ions that should be assigned to Pt oxidation state (Pt^{2+}). The Ni 2p orbital peaks are shown in Fig. 4f. The two peaks at 852.92 eV in Ni $2p_{3/2}$ and 870.60 eV in Ni $2p_{1/2}$ correspond to Ni atoms, and the two peaks at 855.55 eV and 873.52 eV correspond to Ni^{2+} in the oxide formed by natural oxidation of the Ni foam [33]. In the as-prepared PtNi/MoN@C sample, the Pt, Ni, N and Mo contents were 0.44 a.t.%, 1.26 a.t.%, 5.17 a.t.% and 4.74 a.t.% by XPS results. And the actual Pt loading in the PtNi/MoN@C sample is 80.65 μg cm^{-2} by ICP.

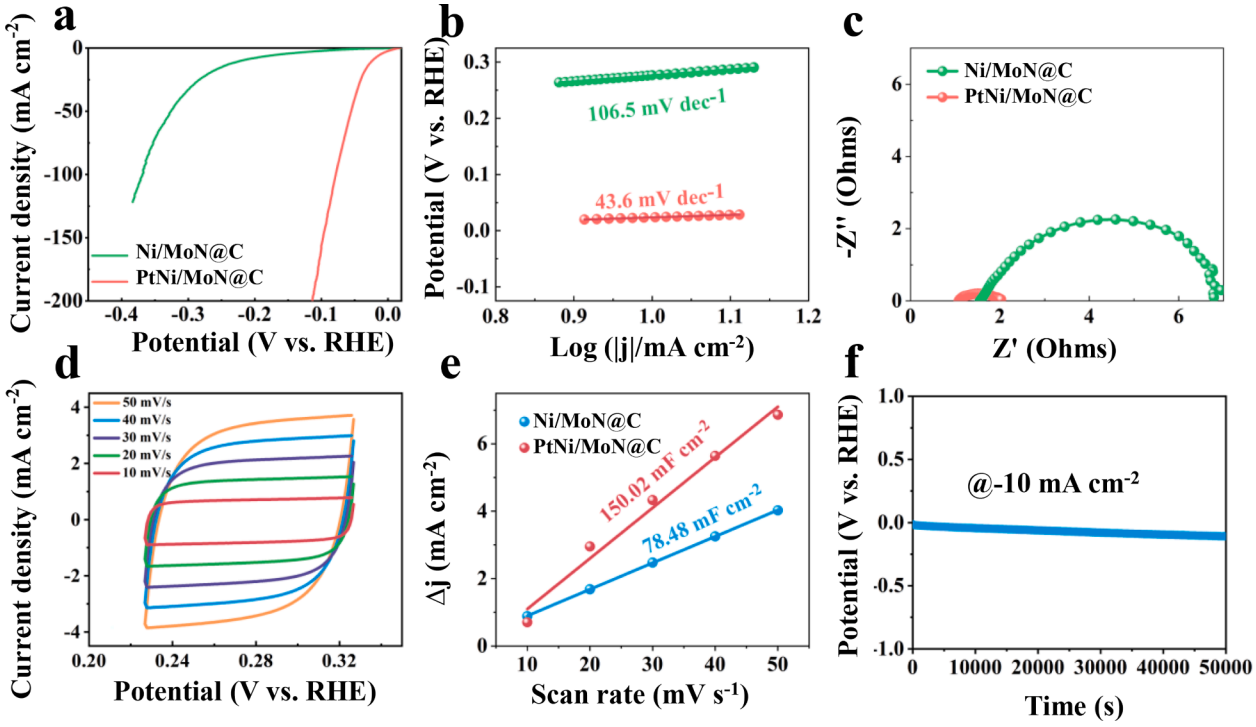


Fig. 5. (a) LSV curves and (b) Tafel plots of the obtained catalysts for HER tests. (c) Nyquist plots of the obtained catalysts. (d) CV curves of PtNi/MoN@C. (e) the calculated electrical double-layer capacitor (C_{dl}) values. (f) Long-time running of PtNi/MoN@C.

The HER tests are carried out in a three-electrode electrochemical system and the electrolyte is 1 M KOH solution. It can be seen that the best electrochemical performance is obtained from the prepared PtNi/MoN@C. Specifically, the overpotential of PtNi/MoN@C can reach 18 mV at a current density of 10 mA cm^{-2}, which is much lower than that of Ni/MoN@C (220 mV). The overpotential is reduced by 202 mV compared to that of Ni/MoN@C, which proves the effectiveness of the designed electrochemical system for the preparation of high performance catalysts. For comparison, the commercial Pt/C electrodes and Ni foam are fabricated and measured shown in Fig. S10 and S11. The overpotential for Ni foam at the current density of 10 mA/cm^2 is 284 mV for HER and Tafel slope is 127.7 mV•dec^{-1}. The kinetic mechanism is further investigated and the Tafel slope is calculated for each sample as shown in Fig. 5b. Comparing the 106.5 mV dec^{-1} of Ni/MoN@C, it can be seen that the Tafel slope of PtNi/MoN@C is smaller at 43.6 mV dec^{-1}, indicating the fastest kinetic behavior of HER. This result shows that the Volmer reaction is the crucial step in the Volmer-Heyrovsky mechanism, which has a significantly higher rate after the introduction of Pt. This may be due to the fact that the complexation of Pt elements adjusts the local electronic structure and reduces the adsorption and desorption energy of hydrogen protons, thus promoting the dissociation of water molecules and the adsorption of H. In order to estimate the electrical resistance in the catalytic reaction as well as the charge transfer capability of the catalyst itself, the electrochemical impedance spectrum (EIS) on the HER side is plotted, as shown in Fig. 5c. It can be seen that the lines of the tested samples are all typical semicircular shapes, and the radius of semicircular of PtNi/MoN@C is much smaller than that of the Ni/MoN@C, which represents the excellent charge transfer capability of PtNi/MoN@C.

Furthermore, the electrochemical surface area (ECSA) of the samples are used to estimate the number of active sites exposed by the electrocatalyst, which can be assessed by calculating the double-layer capacitance (C_{dl}) of the CV curves (Fig. 5d and S12)[34]. Fig. 5e shows that PtNi/MoN@C (150.02 mF cm^{-2}) presents a considerably larger C_{dl} than the Ni/MoN@C (78.48 mF cm^{-2}), indicating that much more active sites are exposed in the HER test due to the introduction of Pt. Then the turnover frequency (TOF) is calculated as follows[35,36]:

$TOF_{H2} = |J| * mA / ECSA * 1C\ s^{-1} / 1000\ mA * 1\ mol\ e^- / 96495.3C * 1\ mol\ H_2 / 4\ mol\ e^- * 6.022 * 10^{23}\ H_2$ molecules / 1 mol H_2.

$= |J| / ECSA * 3.12*10^{15}\ H_2\ s^{-1}$ per mA/cm^2.

At an overpotential of −100 mV, the TOF value of the PtNi/MoN@C electrode is 0.13 s^{-1}, which is 37 times that of Ni/MoN@C (Fig.S13). The electrochemical stability of the system was demonstrated by chronopotentiometry tests. It can be seen that the electrochemical stability of the PtNi/MoN@C is good and the overpotential of the HER do not increase significantly after a long cycle with a current density of −10 mA cm^{-2}, which is also due to the good mechanical contact of the self-supported structure. Besides, the XRD of sample after the stability test

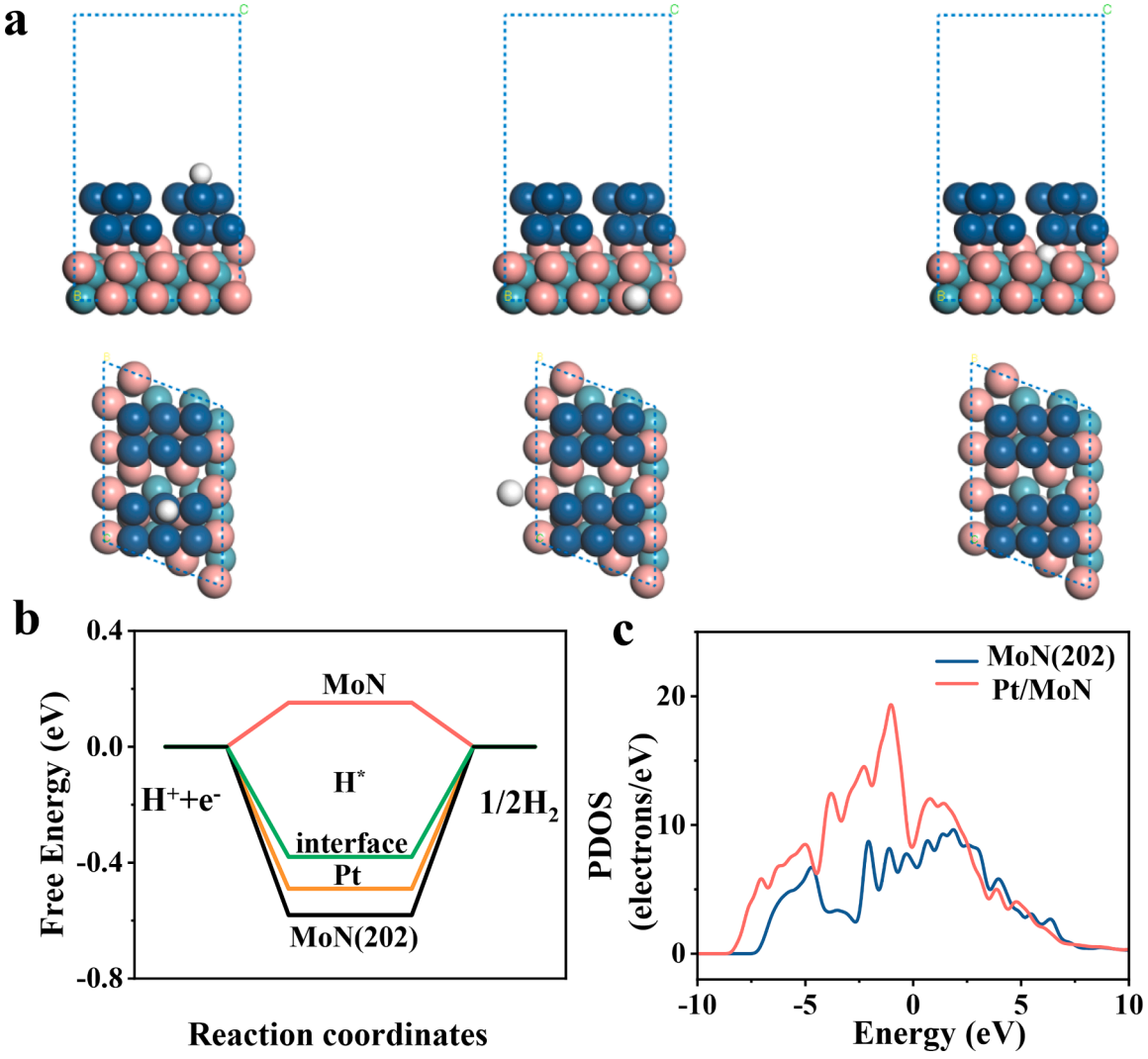


Fig. 6. (a) The atomic models of the H on Pt, H on MoN and H on interface of Pt and MoN. (b) The ΔG_{*H} values of Pt and MoN. (c) The partial density of states (PDOS) of MoN (202) and Pt/MoN.

(Fig.S14) shows the similar to pristine, which indicates a relatively excellent compositional stability.

First-principles calculations are performed on the crystal structure model, as shown in Fig. 6. The free energy of the intermediate (adsorbed hydrogen atom, H*) with respect to the reactant at the selected active sites[37]. Thus, we calculated the $\triangle G_{H^*}$ at different sites of the obtained catalysts. The heterostructure and their specific adsorption sites are shown in Fig. 6a. As shown in Fig. 6b, the calculation results indicate that Pt can effectively reduce the hydrogen adsorption energy at the interface, which is beneficial for the enhancement of HER activity and consistent with the experimental HER performance. And after the introduction of Pt, the total density of states near the Fermi level of MoN (202) increases significantly, which means that the electron transport capability is also significantly improved.

4. Conclusion

In this study, PtNi/MoN@C is synthesized by a simple strategy to obtain stronger interphase effects and significantly improves HER activity. The Pt/MoN nanoparticles are combined with NCNTs with efficient electron conduction, providing the catalyst with an abundance of active sites. As a result, PtNi/MoN@C exhibits a low overpotential of 18 mV in alkaline solutions to deliver -10 mA cm^{-2}, outperforming that of the commercial Pt/C and other reported Mo-based materials such as Co/MoN hetero-interface [38], Co/CoMoN/NF heterostructures [39] and Mo@MoNi alloy [40] etc. Experimental and theoretical studies show that the excellent electrocatalytic performance comes from the synergistic effect of Pt and MoN heterostructure that can increase the number of active sites, and the good combination with carbon nanotubes promotes fast electron conduction. This work provides an approach to the direct compounding of carbon materials with catalysts and has implications for the design of highly efficient HER electrocatalysts.

CRediT authorship contribution statement

Peijia Wang: Conceptualization, Methodology, Writing – original draft. **Yaotian Yan:** Writing – original draft. **Bin Qin:** Data curation. **Zhenyu Ye:** Supervision. **Wei Cai:** Supervision. **Xiaohang Zheng:** Supervision, Funding acquisition.

Declaration of Competing Interest

The authors declare that they have no known competing financial interests or personal relationships that could have appeared to influence the work reported in this paper.

Data availability

Data will be made available on request.

Acknowledgements

The support from the National Natural Science Foundation of China (No.51971083) and the Natural Science Foundation of Heilongjiang Province, China (YQ2020E007). Financially Sponsored by Heilongjiang Touyan Team Program.

Appendix A. Supplementary material

Supplementary data to this article can be found online at https://doi.org/10.1016/j.jcis.2023.07.039.

References

[1] D. Zhao, Z. Zhuang, X. Cao, C. Zhang, Q. Peng, C. Chen, Y. Li, Atomic site electrocatalysts for water splitting, oxygen reduction and selective oxidation, Chem. Soc. Rev. 49 (2020) 2215–2264.
[2] L. Li, P. Wang, Q. Shao, X. Huang, Metallic nanostructures with low dimensionality for electrochemical water splitting, Chem. Soc. Rev. 49 (2020) 3072–3106.
[3] C. Feng, Z.P. Wu, K.W. Huang, J. Ye, H. Zhang, Surface Modification of 2D Photocatalysts for Solar Energy Conversion, Adv. Mater. 34 (2022) 2200180.
[4] S. Sultan, J.N. Tiwari, A.N. Singh, S. Zhumagali, M. Ha, C.W. Myung, P. Thangavel, K.S. Kim, Single atoms and clusters based nanomaterials for hydrogen evolution, oxygen evolution reactions, and full water splitting, Adv. Energy Mater. 9 (2019) 1900624.
[5] J. Song, C. Wei, Z.F. Huang, C. Liu, L. Zeng, X. Wang, Z.J. Xu, A review on fundamentals for designing oxygen evolution electrocatalysts, Chem. Soc. Rev. 49 (2020) 2196–2214.
[6] S. Xu, H. Zhao, T. Li, J. Liang, S. Lu, G. Chen, S. Gao, A.M. Asiri, Q. Wu, X. Sun, Iron-based phosphides as electrocatalysts for the hydrogen evolution reaction: recent advances and future prospects, J. Mater. Chem. A 8 (2020) 19729–19745.
[7] G.A. Gebreslase, M.V. Martínez-Huerta, M.J. Lázaro, Recent progress on bimetallic NiCo and CoFe based electrocatalysts for alkaline oxygen evolution reaction: A review, J. Energy Chem. 67 (2022) 101–137.
[8] W. Huang, C. Su, C. Zhu, T. Bo, S. Zuo, W. Zhou, Y. Ren, Y. Zhang, J. Zhang, M. Rueping, H. Zhang, Isolated electron trap-induced charge accumulation for efficient photocatalytic hydrogen production, Angew. Chem. Int. Ed. 62 (2023) e202304634.
[9] V. Vij, S. Sultan, A.M. Harzandi, A. Meena, J.N. Tiwari, W. Lee, T. Yoon, K.S. Kim, Nickel-based electrocatalysts for energy-related applications: oxygen reduction, oxygen evolution, and hydrogen evolution reactions, ACS Catal. 7 (2017) 7196–7225.
[10] Y. Zhang, C. Han, J. Gao, L. Pan, J. Wu, X. Zhu, J. Zou, NiCo-Based Electrocatalysts for the Alkaline Oxygen Evolution Reaction: A Review, ACS Catal. 11 (2021) 12485–12509.
[11] M. Zhang, Y. Liu, B. Liu, Z. Chen, H. Xu, K. Yan, Trimetallic NiCoFe-Layered Double Hydroxides Nanosheets Efficient for Oxygen Evolution and Highly Selective Oxidation of Biomass-Derived 5-Hydroxymethylfurfural, ACS Catal. 10 (2020) 5179–5189.
[12] Y. Li, Y. Sun, Y. Qin, W. Zhang, L. Wang, M. Luo, H. Yang, S. Guo, Recent Advances on Water-Splitting Electrocatalysis Mediated by Noble-Metal-Based Nanostructured Materials, Adv. Energy Mater. 10 (2019) 1903120.
[13] Z.Y. Yu, Y. Duan, X.Y. Feng, X. Yu, M.R. Gao, S.H. Yu, Clean and Affordable Hydrogen Fuel from Alkaline Water Splitting: Past Recent Progress, and Future Prospects, Adv. Mater. 33 (2021) e2007100.
[14] Y. Liu, G. Chen, R. Ge, K. Pei, C. Song, W. Li, Y. Chen, Y. Zhang, L. Feng, R. Che, Construction of CoNiFe Trimetallic Carbonate Hydroxide Hierarchical Hollow Microflowers with Oxygen Vacancies for Electrocatalytic Water Oxidation, Adv. Funct. Mater. 32 (2022) 2200726.
[15] M. Zhang, Q. Zhang, T. Yu, G. Li, H. Thong, L. Peng, L. Liu, J. Ma, Y. Shen, Z. Shen, J. Daniels, L. Gu, B. Han, L. Chen, J. Li, F. Li, K. Wang, Enhanced electric-field-induced strains in (K, Na)NbO3 piezoelectrics from heterogeneous structures, Mater. Today 46 (2021) 44–53.
[16] N. Yao, R. Meng, J. Su, Z. Fan, P. Zhao, W. Luo, Dual-phase engineering of MoN/Co4N with tailored electronic structure for enhanced hydrogen evolution, Chem. Eng. J. 421 (2021), 127757.
[17] S. Dong, X. Chen, X. Zhang, G. Cui, Nanostructured transition metal nitrides for energy storage and fuel cells, Coordin. Chem. Rev. 257 (2013) 1946–1956.
[18] M. Li, Y. Zhu, H. Wang, C. Wang, N. Pinna, X. Lu, Ni Strongly Coupled with Mo_2C Encapsulated in Nitrogen-Doped Carbon Nanofibers as Robust Bifunctional Catalyst for Overall Water Splitting, Adv. Energy Mater. 9 (2019) 1803185.
[19] Y. Chen, Y. Wang, J. Yu, G. Xiong, H. Niu, Y. Li, D. Sun, X. Zhang, H. Liu, W. Zhou, Underfocus Laser Induced Ni Nanoparticles Embedded Metallic MoN Microrods as Patterned Electrode for Efficient Overall Water Splitting, Adv. Sci. 9 (2022) 2105869.
[20] L. Cai, S. Li, D. Yan, L. Zhou, F. Guo, Q. Sun, Water-Soluble Redox-Active Cage Hosting Polyoxometalates for Selective Desulfurization Catalysis, J. Am. Chem. Soc. 140 (2018) 4869–4876.
[21] H. Jin, C. Guo, X. Liu, J. Liu, A. Vasileff, Y. Jiao, Y. Zheng, S.Z. Qiao, Emerging Two-Dimensional Nanomaterials for Electrocatalysis, Chem. Rev. 118 (2018) 6337–6408.
[22] H. Tabassum, R. Zou, A. Mahmood, Z. Liang, S. Guo, A catalyst-free synthesis of B N co-doped graphene nanostructures with tunable dimensions as highly efficient metal free dual electrocatalysts, J. Mater. Chem. A 4 (2016) 16469–16475.
[23] J. Kwon, H. Han, S. Choi, K. Park, S. Jo, U. Paik, T. Song, Current Status of Self-Supported Catalysts for Robust and Efficient Water Splitting for Commercial Electrolyzer, ChemCatChem 11 (2019) 5898–5912.
[24] Y. Liu, R. Ge, Y. Chen, M. Huang, R. Zhu, W. Li, Y. Liu, L. Feng, R. Che, Urchin-like cobalt hydroxide coupled with N-doped carbon dots hybrid for enhanced electrocatalytic water oxidation, Chem. Eng. J. 420 (2021), 127598.
[25] S. Wang, E. Iyyamperumal, A. Roy, Y. Xue, D. Yu, L. Dai, Vertically aligned BCN nanotubes as efficient metal-free electrocatalysts for the oxygen reduction reaction: a synergetic effect by co-doping with boron and nitrogen, Angew. Chem. Int. Ed. 50 (2011) 11756–11760.
[26] J. Miao, Z. Lang, X. Zhang, W. Kong, O. Peng, Y. Yang, S. Wang, J. Cheng, T. He, A. Amini, Q. Wu, Z. Zheng, Z. Tang, C. Cheng, Polyoxometalate-Derived Hexagonal Molybdenum Nitrides (MXenes) Supported by Boron, Nitrogen Codoped Carbon

Nanotubes for Efficient Electrochemical Hydrogen Evolution from Seawater, Adv. Funct. Mater. 29 (2019) 1805893.
[27] Z. Sun, S. Vijay, H.H. Heenen, A.Y.S. Eng, W. Tu, Y. Zhao, S.W. Koh, P. Gao, Z. W. Seh, K. Chan, H. Li, Catalytic Polysulfide Conversion and Physiochemical Confinement for Lithium-Sulfur Batteries, Adv. Energy Mater. 10 (2020) 1904010.
[28] Y. Liu, G. Yu, G. Li, Y. Sun, T. Asefa, W. Chen, X. Zou, Coupling Mo_2C with Nitrogen-Rich Nanocarbon Leads to Efficient Hydrogen-Evolution Electrocatalytic Sites, Angew. Chem. Int. Ed. 54 (2015) 10752–10757.
[29] L. Wu, F. Zhang, S. Song, M. Ning, Q. Zhu, J. Zhou, G. Gao, Z. Chen, Q. Zhou, X. Xing, T. Tong, Y. Yao, J. Bao, L. Yu, S. Chen, Z. Ren, Efficient Alkaline Water/Seawater Hydrogen Evolution by a Nanorod-Nanoparticle-Structured Ni-MoN Catalyst with Fast Water-Dissociation Kinetics, Adv. Mater. 34 (2022) 2201774.
[30] W. Peng, Z. Wang, R. Lu, Q. Li, Z. Wang, Y. Zhao, L. Xu, L. Mai, Artificial heterointerfaces of defect-rich Ni and amorphous/crystalline MoN enable efficient hydrogen evolution reaction, Chem. Eng. J. 457 (2023), 141173.
[31] X. Shi, A. Wu, H. Yan, L. Zhang, C. Tian, L. Wang, H. Fu, A "MOFs plus MOFs" strategy toward Co–Mo_2N tubes for efficient electrocatalytic overall water splitting, J. Mater. Chem. A 6 (2018) 20100–20109.
[32] C. Chen, L. Jin, L. Hu, T. Zhang, J. He, P. Gu, Q. Xu, J. Lu, Urea-oxidation-assisted electrochemical water splitting for hydrogen production on a bifunctional heterostructure transition metal phosphides combining metal–organic frameworks, J Colloid Interf Sci 628 (2022) 1008–1018.
[33] P. Wang, J. Qi, C. Li, X. Chen, T. Wang, C. Liang, N-Doped Carbon Nanotubes Encapsulating Ni/MoN Heterostructures Grown on Carbon Cloth for Overall Water Splitting, ChemElectroChem 7 (2020) 202000023.
[34] X. Shao, M. Liang, A. Kumar, X. Liu, H. Jin, S. Ajmal, V.Q. Bui, H.T.D. Bui, J. Lee, N.Q. Tran, J. Yu, Y. Cho, M.G. Kim, H. Lee, Amorphization of Metal Nanoparticles by 2D Twisted Polymer for Super Hydrogen Evolution Reaction, Adv. Energy Mater. 12 (2022) 2102257.
[35] J. Kibsgaard, T.F. Jaramillo, Molybdenum phosphosulfide: an active, acid-stable, earth-abundant catalyst for the hydrogen evolution reaction, Angew. Chem. Int. Ed. 53 (2014) 14433–14437.
[36] J. Liu, Z. Wang, D. Zhang, Y. Qin, J. Xiong, J. Lai, L. Wang, Systematic Engineering on Ni-Based Nanocatalysts Effectively Promote Hydrogen Evolution Reaction, Small 18 (2022) e2108072.
[37] H.J. Qiu, Y. Ito, W. Cong, Y. Tan, P. Liu, A. Hirata, T. Fujita, Z. Tang, M. Chen, Nanoporous Graphene with Single-Atom Nickel Dopants: An Efficient and Stable Catalyst for Electrochemical Hydrogen Production, Angew. Chem. Int. Ed. 54 (2015) 14031–14035.
[38] J. Sun, W. Xu, C. Lv, L. Zhang, M. Shakouri, Y. Peng, Q. Wang, X. Yang, D. Yuan, M. Huang, Y. Hu, D. Yang, L. Zhang, Co/MoN hetero-interface nanoflake array with enhanced water dissociation capability achieves the Pt-like hydrogen evolution catalytic performance, Appl. Catal. B: Environ. 286 (2021), 119882.
[39] H. Ma, Z. Chen, Z. Wang, C.V. Singh, Q. Jiang, Interface Engineering of Co/CoMoN/NF Heterostructures for High-Performance Electrochemical Overall Water Splitting, Adv. Sci. 9 (2022) 2105313.
[40] Z. Liu, G. Zhang, J. Bu, W. Ma, B. Yang, H. Zhong, S. Li, T. Wang, J. Zhang, Single-Crystalline Mo-Nanowire-Mediated Directional Growth of High-Index-Faceted MoNi Electrocatalyst for Ultralong-Term Alkaline Hydrogen Evolution, ACS Appl. Mater. Inter 12 (2020) 36259–36267.